Interpreting the $^{13}C/^{12}C$ ratio of carbon dioxide in an urban airshed in the Yangtze River Delta, China

Jiaping Xu[1], Xuhui Lee[1,2*], Wei Xiao[1], Chang Cao[1], Shoudong Liu[1], Xuefa Wen[3], Jingzheng Xu[1], Zhen Zhang[1], Jiayu Zhao[1]

[1]Yale-NUIST Center on Atmospheric Environment, Nanjing University of Information Science & Technology, Nanjing, China

[2]School of Forestry and Environmental Studies, Yale University, New Haven, Connecticut, USA

[3]Key Laboratory of Ecosystem Network Observation and Modeling, Institute of Geographic Sciences and Natural Resources Research, Chinese Academy of Sciences, Beijing, China

* Corresponding author
Dr. Xuhui Lee
Sara Shallenberger Brown Professor
School of Forestry and Environmental Studies, Yale University,
21 Sachem Street, New Haven, Connecticut 06510, USA
Phone: (203)432-6271; Fax: (203)432-5023
E-mail: xuhui.lee@yale.edu

Abstract: Observations of atmospheric CO_2 mole fraction and its ^{13}C isotope composition ($\delta^{13}C$) in urban airsheds provide constraints on the roles of anthropogenic and natural sources in local and regional C cycles. In this study, we report observations of these quantities in Nanjing at hourly intervals from March 2013 to August 2015 using a laser-based optical instrument. Nanjing is the second largest city located in the highly industrialized Yangtze River Delta (YRD), Eastern China. The mean CO_2 mole fraction and $\delta^{13}C$ were 439.7 ppm and -8.48‰ over this observational period. The peak monthly mean $\delta^{13}C$ (-7.44‰, July 2013) was 0.74‰ higher than that observed at the Mount Waliguan. The highly enriched ^{13}C signal was partly attributed to the influence of cement production in the region. By applying the Miller-Tans method to nighttime and daytime observations to represent signals from the city of Nanjing and the YRD, respectively, we showed that the ^{13}C signal of C sources in the Nanjing Municipality was 0.48‰ lower than that in the YRD. Flux partitioning calculations revealed that natural ecosystems in the YRD were a negligibly small sink of atmospheric CO_2, consistent with the Carbon Tracker inverse modeling result.

Keywords: urban areas; CO_2 flux; Industrial process; Carbon isotope; In-situ observation

41 **1 Introduction**

42 Atmospheric CO_2 sources and sinks in urban areas consist mainly of plant uptake and release
43 and fossil fuel combustion. These contributors have unique ^{13}C isotopic signatures. City
44 clusters are human-dominated systems with high carbon emission intensity, contributing over
45 70% of the total anthropogenic CO_2 to the atmosphere (Satterthwaite 2008). Previous urban
46 isotopic studies emphasize carbon emissions from fossil combustion (Zondervan and Meijer
47 1996, Pataki et al. 2003, Zimnoch et al. 2004, Affek and Eiler 2006, Newman et al. 2008).
48 Relatively little attention is given to the isotopic signature of carbon dioxide released by
49 cement production, which is much heavier than that of fossil fuel origin (Andres et al. 1994).
50 Likewise, the CO_2 emitted from burning of minerals in non-energy consumption industrial
51 processes, such as iron and steel production, has higher ^{13}C composition than that of fossil
52 fuel (Table 1, Widory 2006). In China, cement production and industrial processes contribute
53 13% of the total anthropogenic CO_2 emission (Mu et al. 2013). Many of these industrial
54 activities occur in or near urban areas. So far, little is known about their roles in the
55 atmospheric $\delta^{13}C$ budget.

56 One scientific motivation for quantifying the ^{13}C signature of atmospheric CO_2 is that it
57 provides constraints that allow partitioning of the net surface flux into component fluxes
58 (Farquhar and Lloyd 1993, Yakir and Sternberg 2000, Pataki et al. 2003). The ^{13}C-based
59 partitioning method has been used primarily for vegetation ecosystems, such as forests
60 (Lloyd et al. 1996, Lloyd et al. 2001, Ometto, et al. 2006, Zobitz et al. 2008), grasses (Ometto
61 et al. 2002, Pataki et al. 2003), and crops (Leavitt et al. 1995, Griffis et al. 2005). The
62 approach has also been used in a limited number of urban studies (Pataki et al. 2003,

63 Zimnoch et al. 2004, Newman et al. 2008, Jasek et al. 2014). Compared with vegetation
64 ecosystems, urban ecosystems have more complex CO_2 source configuration. We must
65 consider both natural sources (plants and soils) and anthropogenic sources (fossil combustion
66 and non-energy industrial processes) and the fact that the degree of mixing of urban air with
67 the free troposphere and the air outside the urban boundary varies diurnally and seasonally.
68 Anthropogenic emissions are hard to quantify because they depend on multiple factors
69 including city size, population density, fossil mix, and climate.

70 One of the first measurements of the carbon isotope composition of CO_2 in an urban
71 atmosphere was made by Friedman and Irsa (1967). Since then, a few more experiments have
72 been conducted in urban environments. The data collected have been used to partition CO_2
73 contributors (Koerner and Klopatek 2002, Clark-Thorne and Yapp 2003), to quantify diurnal
74 variations in the CO_2 mole fraction and its $\delta^{13}C$ in urban air (Zimnoch et al. 2004, Guha and
75 Ghosh 2010) and across urban to rural gradients (Lichtfouse et al. 2003, Pataki et al. 2007),
76 and variations among different land uses in urban areas (Clark-Thorne and Yapp 2003,
77 Widory and Javoy 2003). The isotopic data reveal insights into energy consumption patterns
78 (Widory and Javoy 2003, Bush et al. 2007), impacts of meteorology including temperature
79 (Clark-Thorne and Yapp 2003, Zimnoch et al. 2004), atmospheric stability (Pataki et al. 2005)
80 and wind (Clark-Thorne and Yapp 2003) on urban carbon cycling, and the role of vegetation
81 phenology (Ehleringer et al. 2002, Takahashi et al. 2002, Wang and Pataki 2012). The
82 analytical technique employed in these studies is mainly based on mass-spectrometry (MS).
83 Because sample collection, preparation and analysis are labor intensive, the majority of these
84 studies are limited to short campaigns (less than 60 days).

In recent years, the development of isotope ratio infrared spectroscopy (IRIS) and on-line calibration technology provides a new solution for long-term in-situ observation of the CO_2 mole fraction and its $\delta^{13}C$ at high frequencies (1 Hz to 1 hour; Pataki et al. 2006, Griffis. 2013, Gorski et al. 2015). Compared with the MS method, IRIS can capture diurnal or even shorter temporal variations with relatively high accuracy, enabling us to understand how anthropogenic emissions change atmopheric CO_2 at highly resolved temporal and spatial scales. Nevertheless, application of the IRIS technology in urban monitoring is still limited in terms of cities covered and measurement duration: less than 35 days in McManus et al. (2002), Pataki et al. 2006 and Wada et al. (2011) and 3 seasons in Moore and Jacobson (2015). Only one published study has presented data that spans one full annual cycle (Pang et al. 2016).

Simultaneous measurement of atmospheric CO_2 concentration and its isotopic composition is used to determine the overall isotopic signature of local surface sources $\delta^{13}C_S$. All published urban studies to date have deployed the Keeling plot method (Keeling 1958, Keeling 1961) for the determination of $\delta^{13}C_S$. In this approach, a linear relationship is established between $\delta^{13}C$ and the reciprocal of the CO_2 mole fraction from the observed time series, and the intercept of the linear regression is taken as the isotopic composition of the local CO_2 emissions. The method assumes that the isotopic signature of the sources is invariant with time. It also assumes that changes in the CO_2 mole fraction and in $\delta^{13}C$ are attributed only to the surface sources and are unaffected by regional carbon sources (Pataki et al. 2003). However, these assumptions do not strictly hold in an urban environment because the intensity of traffic emissions varies strongly through the diurnal cycle (McDonald et al.

2014), and therefore the composition of the surface source varies, and its ^{13}C signature cannot be assumed constant. In addition, because of strong atmospheric mixing in the daytime convective boundary layer, the background air in the upper troposphere can be easily entrained to the surface layer, mixing the CO_2 that originates from regional sources with that emitted locally in the urban airshed.

Miller and Tans (2003) propose that $\delta^{13}C_S$ be determined as the slope of the linear relationship

$$\delta_a C_a - \delta_b C_b = \delta^{13} C_s (C_a - C_b) \quad (1)$$

where C_a is CO_2 mole fraction in urban air, C_b is CO_2 mole fraction in a background site, δ_a is ^{13}C isotopic composition of C_a, and δ_b is ^{13}C isotopic composition of C_b. We argue that because this approach takes into account the fact the background atmosphere varies, it is more suitable than the Keeling method for inferring $\delta^{13}C_S$ from the observations made in the urban area with complex emission sources. The method has been applied to local and regional carbon budget studies in nonurban settings (Miller et al. 2003). Here we extend the method to an urban environment.

In this study, we report the results of long-term (30 months) continuous measurement of atmospheric CO_2 mole fraction and its $\delta^{13}C$ at a suburban site in Nanjing using an IRIS instrument. Nanjing is the second largest city in the Yangtze River Delta (YRD), Eastern China, with a build-up area of 753 km^2 and a population of 8.2 million. Geographically, the YRD includes the provinces of Jiangsu, Zhejiang and Anhui and the Shanghai municipality (29.04°-33.41°N, 118.33°-122.95°E) with a population of 1.9 hundred million. The YRD is influenced by subtropical moist monsoon climate. The mean annual temperature is about

15°C and the annual precipitation is between 1000 mm and 1800 mm. The main vegetation types, all of which are C3 species. The YRD is the most industrialized region in China and had a higher urban land fraction of 10.8% as of 2014 than the global mean (2.4%, Akbari et al. 2009). In 2014, more than 220 large cement production factories (daily output exceeding 1000 tons) were located in the YRD (China Cement, 2016), contributing about 20% of the national cement output.

The objectives of this study are (1) to characterize the atmospheric $\delta^{13}C$ diurnal, seasonal and annual variations in this urban environment, in a region where such measurement is nonexistent, (2) to investigate the influence of cement production on atmospheric $\delta^{13}C$, (3) to evaluate the performance of the Keeling plot and the Miller-Tans method for determining $\delta^{13}C_S$, and (4) to explore the utility of the isotopic constraints for inferring the net surface flux and the plant CO_2 flux in Nanjing and in the YRD.

2 Methods

2.1 Atmospheric observation

An IRIS analyzer (model G1101-i, Picarro Inc., Sunnyvale, CA) was used to measure atmospheric CO_2 mole fraction and its ^{13}C isotope composition ($\delta^{13}C$) continuously from February 2013 to August 2015. The analyzer was housed on the 9th floor of our laboratory building on the campus of Nanjing University of Information, Science and Technology (NUIST, 32°12'N, 118°43'E), in the northern suburb of Nanjing, at a linear distance of 20 km to the city center. The instrument inlet was at a height of 34 m above the ground. There was no anthropogenic CO_2 source in the 3 km radius except for a commuting road located about

300 m east of the observation site. The nearest industrial complex, the Nanjing Iron & Steel Group Co. Ltd. and the Nanjing Chemical Industry Group, was located ~5 km to the south of the site. The measurement was made at 0.3 Hz and at an air flow rate of 30 mL min^{-1} at standard temperature and pressure. One three-way solenoid valve was combined with two two-way solenoid valves, so the analyzer could be switched for atmospheric sampling and for sampling of two standard gases. Calibration was carried out every 3 h by sampling each standard gas for 5 minutes following the procedure of Bowling et al. (2003) and Wen et al. (2013). (To avoid transient effects, only the data collected in the last 2 minutes was used.) Table 1 lists the concentrations and their isotopic compositions of the standard gases used in this study. The CO_2 mole fraction of the standard gases was traceable to the WMO 2007 scale reported by the Central Calibration Laboratory of the World Meteorological Organization and their $\delta^{13}C$ was based on the NBS-19 and the NBS20 standards of NIST. The ambient measurement was averaged to hourly intervals. The isotopic composition was expressed in the delta notation ($\delta^{13}C$) in reference to the VPDB scale.

The typical 5-min measurement precision is 0.3‰ for $\delta^{13}C$ and 0.05 ppm for CO_2 mole fraction according to the instrument manufacturer. Our own Allan variance analysis revealed a precision of 0.05‰ for $\delta^{13}C$ and 0.07 ppm for CO_2 mole fraction at the hourly averaging interval. We did not adopt the strict filtering technique used for background sites (Thoning et al. 1989) because of high natural variations in urban airsheds. We removed 40 3-minute data points during the transient periods after calibration gas changes. Additionally, data were removed if hourly CO_2 mole fraction was lower than 390 ppm or $\delta^{13}C$ were out of the range between -15‰ and -5.5‰.

The $\delta^{13}C$ measured by the analyzer in high humidity conditions suffers a high bias error due to spectral broadening and direct spectral interference (Rella 2011) . To correct for the humidity interference, we carried out two tests using a dew-point generator (model 610, LI-COR, Inc., Lincoln, NE). A CO_2 standard gas (secondary standard gas, 439 ppm in test one and 488 ppm in test two, balanced by dry air) was fed into the dew-point generator. The outlet of the dew-point generator was connected with a 3-way union with one end linked to the inlet of the analyzer and the other open to the room. The humidity level of the air coming out of the dew point generator was regulated at eight levels in a dew-point temperature range of 1 and 30°C, giving a humidity ranging from 0.66 V% to 4.26 V%. Because the ^{13}C composition of the standard gas was constant, any observed variations were caused by the humidity artifact. We found that no correction was needed for our analyzer if the humidity was below 2.03%. Above this humidity level, the measurement was biased high by 0.46‰ for every 1% increase in the water vapor volume or mole fraction (Figure 1). The two tests, taken eight months apart, yielded essentially the same result. The correction equation is

$$\delta^{13}C = \delta^{13}C_{true} \qquad H \leq 2.03\% \qquad (2a)$$

$$\delta^{13}C = \delta^{13}C_{true} + 0.46(H - 2.03) \qquad H > 2.03\% \qquad (2b)$$

where H is water vapor volume mole fraction in percent, $\delta^{13}C$ is the measured isotopic composition (after the two-point calibration), and $\delta^{13}C_{true}$ is the true isotopic composition. The ambient humidity varied from 0.16 to 3.64 V% during the measurement period. About 35% of the observations exceeded the threshold humidity of 2.03%V and required correction. The largest hourly correction was 0.74‰. In the following, all the data has been corrected for the humidity interference.

2.2 The isotopic composition ($\delta^{13}C_S$) of surface sources

We applied the Miller-Tans method to the data collected in daytime hours (10:00 to 16:00 local time; Equation 1) to represent YRD and to the data collected during nighttime hours (22:00-6:00 local time) to represent Nanjing. The slope was obtained by linear regression of (C_a-C_b) against ($\delta_a C_a$-$\delta_b C_b$) over monthly intervals. The monthly mean CO_2 mole fraction and the isotopic composition of the background air were those observed at Mount Waliguan (WLG, 36°17'N, 100°54'E, 3816 m above the mean sea level; Zhou et al., 2005) located at the northeastern edge of the Tibetan Plateau, the closest upwind background station for Nanjing. Because the WLG data were not available for 2015 at the time of this analysis, we fitted the WLG data of both CO_2 and $\delta^{13}C$ with a four-harmonic quadratic function (Thoning et al. 1989) using the dataset from 2000 to 2014, and then used the function to estimate the monthly $\delta^{13}C_b$ and C_b values for 2015.

The selection of a background site is a critical issue when applying the Miller-Tans method (Ballantyne et al., 2011 & 2010, Turnbull et al., 2015). Ideally, the background site should not be affected by local and regional emission and should lie in the upwind direction of the observation site. Based on these criteria, we chose WLG as the background site for our analysis.

We interpreted the daytime results to represent the influence of surface sources in the YRD region and the nighttime results to represent the influence of surface sources in the Nanjing. The vigorous turbulent exchange in the daytime boundary layer diminishes the role of local sources in the measured concentration and isotopic ratio. In other words, the daytime

measurement has a much larger source footprint than the size of the urban land itself or the footprint of the nighttime measurement. In contrast, the buildup of CO_2 at night is primarily the result of sources in the city (Shen et al. 2014), so we considered the $\delta^{13}C_S$ determined from the nighttime observations to represent the signal of the sources located in the city. Admittedly, this interpretation of daytime versus nighttime source areas is a simplification because the actual source area also depends on thermal stratification and boundary layer wind. Nevertheless, it is supported by a trajectory analysis and by an analysis of the atmospheric methane to CO_2 emissions ratio (Shen et al. 2014).

2.3 Inventory of anthropogenic sources

We calculated the anthropogenic CO_2 fluxes from energy consumption and industrial process following the SCOPE 1 procedure issued by the International Council for Local Environmental Initiatives (ICLEI, 2008). The procedure considers only emissions from sources that lie within the geographic boundary of investigation. The energy consumption source consists of direct emissions from the three main energy consumption sectors (industry, transport, and household). We ignored the commerce sector here because the main energy consumption in this sector in Nanjing and in the YRD was electric power generated by coal and coal consumption which was already considered in SCOPE 1. The amounts of CO_2 emission were estimated with the IPCC methodology adopting the emission factors for each fossil fuel type recommended by IPCC. The calculations were done separately for the YRD region and for the Nanjing municipality. Because no statistical data were available for energy consumption in the transport sector in Nanjing, the CO_2 emission from the transport sector

was deduced according to vehicle number, average annual driving distance and coefficients of fuel economy (Bi et al. 2011). We obtained the data on energy consumption from official sources (CESY 2013, CSY 2013, NSY, 2013).

The non-energy industrial processes included cement, raw iron, crude steel, and ammonia synthesis processes. In the YRD, the data were available at monthly intervals. For the city of Nanjing, only annual statistics were available.

2.4 Partitioning the net surface flux

We partitioned the surface CO_2 flux (F_S) into three component fluxes according to the following mass conservation equations

$$F_S = F_F + F_C + F_P \quad (4)$$

$$\delta^{13}C_S F_S = \delta^{13}C_F F_F + \delta^{13}C_C F_C + \delta^{13}C_P F_P \quad (5)$$

where F_F is the flux from fossil fuel combustion and industrial emission except cement production (termed "fossil plus"), F_C is the flux due to cement production, F_P is the biological flux, and $\delta^{13}C_F$, $\delta^{13}C_C$, and $\delta^{13}C_p$ are the ^{13}C isotope composition of F_F, F_C and F_P, respectively. These fluxes are obtained by dividing the total emission by the surface area within the geographic boundary of Nanjing or YRD, having dimensions of mg CO^2 $m^{-2}s^{-1}$. We separated the cement source from other non-energy consumption industrial processes because its isotopic signature is much higher. In these equations, the monthly net surface flux (F_S) and the biological flux (F_P) are unknowns to be solved, and all other terms are either provided by the atmospheric measurement or by the inventory calculation. The partitioning

analysis was done for both Nanjing and the YRD using the nighttime and daytime observations, respectively.

The $\delta^{13}C_F$ was weighted average of the $\delta^{13}C$ signal of individual fuel types and industrial processes (Widory 2006; Table 2). The isotopic composition of CO_2 from cement production is provided by Tans (1981) and Anders (1994). We adapt a value of (-28.2‰) for $\delta^{13}C_P$ for the YRD and Nanjing, on account of a linear relationship between $\delta^{13}C_P$ and tree age (Fessenden and Ehleringer 2002), a typical tree age in this region (40 years) and an U-shaped relationship between $\delta^{13}C_P$ and annual precipitation (Pataki et al. 2007). Our $\delta^{13}C_P$ is more negative than that reported for a boreal forest (-26.2‰; Pataki et al. 2007) but is in closer agreement with the value reported for a Ginkgo tree in Nanjing (-29.3‰; Sun et al. 2003). A summary of the isotopic compositions of the three source categories is given in Table 3.

To partition the nighttime flux for Nanjing, we assumed that the nighttime F_F was 20% of the daily value. The parameter 20% was determined by the diurnal variation of the CO_2 flux observed with an eddy covariance system in Nanjing (Bai 2011) and in several other cities (Coutts et al. 2007, Song and Wang. 2011, Liu et al. 2012). At night, most of the factories in the city were closed and the traffic flow was reduced to about 80% of the daytime volume (Yang et al. 2011).

3. Results

3.1. Temporal variations in the CO_2 mole fraction and $\delta^{13}C$

The monthly CO_2 mole fraction during the summer was slightly lower than in the other seasons (Figure 2). The mean mole fraction was 446.7 ppm and 431.1 ppm for January and

July, respectively, giving a seasonal amplitude of 15.6 ppm. The mean CO_2 mole fraction was 439.7 ppm during the whole experimental period (March 2013 to August 2015), which is 40.6 ppm higher than value observed and estimated at WLG for the same period. In 2014, the calendar year with complete data coverage, the mean CO_2 mole fraction was 441.2 ppm, which is 42.5 ppm higher than the WLG value for the same year.

The ^{13}C composition of atmospheric CO_2 displayed a larger seasonal cycle than the mole fraction (Figure 2). The monthly mean value was -9.07‰ and -7.63‰ for January and July, respectively, with a seasonal amplitude of 1.44‰. The mean value for the whole experimental period was -8.48‰, which is the same as the WLG value (-8.48‰). The summertime (June-August) $\delta^{13}C$ was 0.39‰ more enriched than the WLG background value.

The strongest diurnal variation in the CO_2 mole fraction was observed in the autumn season and the weakest in the winter season, with a diurnal amplitude of 27.9 ppm and 13.4 ppm, respectively (Figure 3). In the summer season, the peak value was observed at 07:00 and the lowest value at 19:00. Contrary to the CO_2 mole fraction, $\delta^{13}C$ showed the lowest value in the early morning and the highest value in the afternoon in all the four seasons. The diurnal amplitude was 1.36‰ in the summer and 0.66‰ in the winter.

3.2 Isotopic composition of the surface sources ($\delta^{13}C_S$)

Applying the Miller-Tans approach to the whole experimental period yielded an apparent source signature of -24.75±0.26‰ (mean ± 95% confidence bound) for sources in the YRD (Figure 4) and -24.24±0.21‰ for sources in Nanjing (Figure 5). Strictly, this method is not accurate when applied over such an extensive period because the source signature varies

seasonally, violating the condition of constant source signal under which the method can be used. So these data plots are meant more to show the range of variations of the hourly observations than for determining the true annual mean source signatures.

Figure 6 shows the monthly ^{13}C signature calculated with the Miller-Tans method for the daytime and nighttime. The reader is reminded here that the results obtained for the daytime and the nighttime period represent sources in the YRD and in Nanjing, respectively. During the two and a half years of observation, the monthly $\delta^{13}C_S$ was lower in the winter and higher in the summer. The sources in the YRD had higher ^{13}C compositions than those in in Nanjing. The January mean value (mean of January 2014 and January 2015) was -24.13‰ and -24.78‰, and the mean value of the three August months was -20.67‰ and -22.76‰ for the YRD and Nanjing, respectively. The mean value of the whole observational period was -23.26‰ and -23.72‰ for the YRD and Nanjing, respectively. These mean values based on the monthly analysis were 1.49‰ and 0.52‰ greater than the apparent source signatures derived from the application of the Miller-Tans method to the whole dataset (Figures 4 and 5). The monthly $\delta^{13}C_S$ for the YRD (Figure 6) was highly correlated with the monthly atmospheric $\delta^{13}C$ (Figure 2; linear correlation = 0.63, n = 30, $p < 0.001$). The correlation between the monthly $\delta^{13}C_S$ for Nanjing and the monthly atmospheric $\delta^{13}C$ was not as strong (linear correlation = 0.26, n = 30, p = 0.22).

3.3 Inventory data for anthropogenic sources

The emission strength of anthropogenic sources and their isotopic signature were calculated with the inventory method described in section 2.3. In the YRD, coal combustion was by far

the largest source of anthropogenic CO_2, contributing 70% of the overall "fossil-plus" emission (Table 2). Here the "fossil-plus" emission includes contributions from all forms of fossil fuel and from non-cement industrial processes. The second and third largest source were ammonia synthesis and pig iron, with fractional contributions of about 9%. The "fossil-plus" source contribution to the total anthropogenic emission was 91%, with the remaining 9% contributed by cement production (Table 2).

In the Nanjing municipality, the fractional contribution of coal to the "fossil-plus" total was 52%, lower than that for the YRD, and the other three major sources were ammonia synthesis (16%), pig iron (13%), and gasoline (11%). The fractional contribution of fuel-plus sources to the total anthropogenic emission was 96.4% and the fractional contribution of cement production was 3.6% (Table 2). The isotopic signature of the "fossil-plus" sources was 0.35‰ lower for Nanjing than for the YRD.

The overall effective isotopic signature of the anthropogenic sources weighted by the source contributions was also lower for Nanjing than for the YRD (Table 3). The difference was 1.76‰ and was a result of lower fractional contributions in Nanjing of coal combustion and cement production, which have relatively high ^{13}C contents, and a higher fractional contribution of natural gas, which is the fuel type with the lowest ^{13}C content.

3.4. CO_2 fluxes in YRD and Nanjing

Figure 7 shows the biological flux F_P and surface flux F_S calculated from the mass balance, and the cement flux F_C and "fossil-plus" F_F. The F_P flux obtained with the isotopic partitioning method for the YRD agreed with the seasonal phenology expected for plants in

this region. It was slightly negative in the summer and positive in the winter, indicating uptake and release, respectively. The annual mean daytime biological flux was -0.01 mg $m^{-2}s^{-1}$ in the YRD in the calendar year 2014. The net surface flux F_S was 0.16 mg $m^{-2}s^{-1}$.

In Nanjing, the biological flux was positive throughout the year. This is because the partitioning was done for the night hours when the natural ecosystems were a source of CO_2 due to autotrophic and heterotrophic respiration. The flux was greater in the summer than in the winter (Figure 8). The annual mean nighttime biological flux for the calendar year 2014 was 0.03 mg $m^{-2}s^{-1}$. The nighttime surface flux was 0.16 mg $m^{-2}s^{-1}$.

4 Discussion

4.1 CO_2 mole fraction and $\delta^{13}C$ seasonality

The atmospheric CO_2 mole fraction observed in Nanjing showed very small seasonal variation (summer versus winter difference of 7.9 ppm, July versus January difference of 15.6 ppm), in comparison with the data published for other cities. The CO_2 mole fraction difference between the cold and the warm season is about 66 ppm in Phoenix, USA (Idso et al. 2002). In Salt Lake City, USA, the CO_2 mole fraction in the summer is about 31 ppm lower than in the winter (Pataki et al., 2003). In Chicago, USA, the CO_2 mole fraction varied from 397 ppm in August 2011 to 427 ppm in January 2012, showing a seasonal amplitude of 30 ppm (Moore and Jacobson 2015). In Beijing, China, the seasonal variation of atmospheric CO_2 mole fraction is about 64.5 ppm (August versus January; Pang et al. 2016). However, a similar small seasonal amplitude of 5 ppm CO_2 was observed in Pasadena, USA during 2006

to 2013, which was consistence with the seasonal variation of background and emission from fossil fuel combustion (Miller et al. 2016).

Several factors contributed to the weak seasonality in Nanjing. The climate in the YRD is relatively mild. The governmental energy policy prohibits winter heating in public buildings. Most residential buildings also lack space heating in the winter. This is in contrast to energy use patterns in northern cities in China and elsewhere. In London, UK, natural gas usage in the winter heating season is 29% greater than in the non-heating autumn season (Helfter et al. 2011). In Salt Lake City, USA, energy consumption in the winter was 41% greater than in the summer (Bush et al, 2007). A similar seasonal trend of energy consumption has also been reported for Beijing (Pang et al, 2016). In Chicago, natural gas usage varied 70% to 80% in winter and about 50% in summer (Moore and Jacobson 2015). The weak energy use seasonality in the YRD partially explains why the observed CO_2 mole fraction had a smaller seasonal amplitude (Figure 2) than reported for other northern cities.

The weak seasonality of the observed mole fraction was also related to the low vegetation cover in the YRD and in Nanjing. The forest cover ratio is about 35% in Nanjing and in the YRD, and the overall vegetation cover (forest plus other vegetation types) ratio in the major cities in the YRD is lower than 45% (CESY, 2013; CSY, 2013). For comparison, the vegetation cover ratio is 56% in Salt Lake City (Pataki et al. 2009) and 44% in Chicago (Rose et al. 2003). Dense vegetation is known to deplete atmospheric CO_2 in the summer season via photosynthetic uptake, amplifying the CO_2 seasonal amplitude.

Our $\delta^{13}C$ seasonal amplitude (January versus July difference 1.44‰) was 4 times the amplitude observed or estimated at WLG (Figure 2) but agreed with those reported by most

391 urban studies. For comparison, the seasonal amplitude of $\delta^{13}C_a$ in Bangalore, India, was 0.89
392 to 1.32‰ (Guha and Ghosh 2015). Similar amplitudes have also been reported for Chicago
393 (January versus August difference 1.25‰; Moore and Jacobson, 2015) and Beijing (2.13‰;
394 Pang et al. 2016). In Salt Lake City, the seasonal amplitude of $\delta^{13}C$ was approximately 1.6‰
395 because of much more natural gas consumption for heating in the winter than in the summer
396 (Pataki et al. 2006).
397
398 **4.2 Influences of cement production on atmospheric $\delta^{13}C$**
399 The high summer $\delta^{13}C$ was one of the most unique characteristics at our site. The daytime
400 $\delta^{13}C$ reached -6.90‰ in July 2013 and -7.21‰ in August 2014, which were 1.28‰ and
401 0.95‰ higher than the WLG values. The highest monthly mean $\delta^{13}C$ occurred in July: -
402 7.44‰ in July 2013, -7.99‰ in July 2014 and -7.46‰ in July 2015. These values were
403 0.74‰, 0.16‰ and 0.77‰ higher than the WLG value reported for the same months.
404 The high July values observed at our site cannot be fully explained by CO_2 removal by
405 plant photosynthesis. Photosynthesis and respiration are the two processes that dominate the
406 ^{13}C seasonality in plant-dominated landscapes, leading to higher $\delta^{13}C$ values in the summer
407 and lower values in the winter. For example, in Park Falls, Wisconsin, USA, a site in a
408 heavily-forested landscape, $\delta^{13}C$ was -7.75‰ in August 2011 and -8.77‰ in February 2012
409 (Moore and Jacobson, 2015). For comparison, $\delta^{13}C$ was -8.24‰ and -8.38‰ at the Mauna
410 Loa Observatory and -8.02‰ and -8.66‰ at WLG in these two months, respectively. In other
411 words, the photosynthetic effect raised the August $\delta^{13}C$ by 0.5‰ above the background value,
412 a smaller enrichment than observed at our site. Because of the low vegetation fraction, the

summer photosynthetic CO_2 uptake in the YRD and in Nanjing should be lower than at Park Falls. According to the Carbon Tracker inversion analysis (Peters et al. 2007), the net ecosystem production at the grid point where Parks Fall is located is -0.201 mg $m^{-2}s^{-1}$ in July, 2014 but is only -0.059 mg $m^{-2}s^{-1}$ at the grid point corresponding to the YRD region. We would expect from the photosynthetic effect alone that the summertime ^{13}C enrichment at our site to be smaller, not greater than that observed at Parks Fall.

Furthermore, in a human-dominated landscape, the plant photosynthetic enhancement of ^{13}C is offset by the CO_2 from fossil fuel combustion which has low ^{13}C contents. In Chicago, the monthly $\delta^{13}C$ peaked in August at -8.29‰ during the calendar year 2011, which is 0.05‰ lower than the WLG for the same month. Similarly, in Beijing, the monthly $\delta^{13}C$ peaked at -9.49‰ in August 2014, which is 1.23‰ lower than the WLG value for the same month.

We suggest that cement production was the contributing factor responsible for the high $\delta^{13}C$ values in the summer. The evidence supporting this interpretation is provided by data in Table 3 and Figure 7. The $\delta^{13}C$ signal of anthropogenic CO_2 in the YRD would be -26.42‰ without cement production and increased to -23.71‰ after inclusion of the cement source (Table 3). This $\delta^{13}C$ value is much higher than those reported for other urban lands, such as -30.7‰ for Los Angeles, USA (Newman et al. 2008) and about -31‰ for Salt Lake City, USA (Bush et al. 2007). The overall surface source signal derived from atmospheric measurements (Figure 6, -23.26‰ and -23.72‰ for the YRD and Nanjing, respectively) was also more enriched than those obtained from atmospheric measurements in other cities, such as -28.1±0.8‰ for Chicago in August and September (Moore and Jacobson, 2015), -32.4‰ to -27.4‰ for Salt Lake City in the growing season (Pataki et al. 2003), -27.0‰ for Beijing in

435 the winter heating season (Pang et al. 2016), and -29.3‰ for Los Angeles, USA (Newman et
436 al. 2008).

437 The influence of cement production on atmospheric $\delta^{13}C$ has also been suggested for at
438 least two other urban sites. In Bangalore, India, $\delta^{13}C$ is 0.05‰ higher than that observed at an
439 island station in the Indian Ocean, and cement production in southern India is offered as a
440 reason to explain the enrichment of urban $\delta^{13}C$ (Guha and Ghosh 2015). The other urban site
441 is Beijing, China, where the $\delta^{13}C$ measurement may have been influenced by cement factories
442 outside the city (Ren et al. 2015, Pang et al. 2016).

443

444 **4.3 Net surface and biological fluxes in the YRD**

445 As a human-dominated landscape, the YRD was a net source of CO_2 on the monthly scale
446 even in the growing season (F_S, Figure 7). The seasonal trends of the net surface flux F_S and
447 the biological flux F_P were highly correlated with each other because the anthropogenic
448 source strengths were almost constant. The mean F_S between March 2013 and February 2015
449 was 0.17 mg $m^{-2}s^{-1}$, which consisted of 0.16 mg $m^{-2}s^{-1}$ from fossil combustion and industrial
450 processes, 0.02 mg $m^{-2}s^{-1}$ from cement production and -0.01 mg $m^{-2}s^{-1}$ from biological
451 activities. The total anthropogenic CO_2 flux was 0.18 mg $m^{-2}s^{-1}$ in the YRD, a 67% increase
452 from the value of 0.10 mg $m^{-2}s^{-1}$ reported for 2009 (Shen et al. 2014). From 2009 to 2012, the
453 GDP increased by 56% according to the National Statistic Yearbook.

454 For comparison, we extracted the flux data from the Carbon Tracker database for the 6
455 by 6 pixels that cover the YRD region. The results show that the mean daytime (11:00 to
456 17:00 local time) biological flux is slightly negative at -0.014 mg $m^{-2}s^{-1}$ for 2014 (Peter et al.

2007). Our estimate of F_P for 2014 also indicates that the region was a negligibly small biological sink of CO_2 (-0.009 mg $m^{-2}s^{-1}$).

We conducted Monte Carlo simulations to assess the sensitivity of the partitioned fluxes to uncertainties in $\delta^{13}C_P$ and $\delta^{13}C_F$. Errors in these parameters were assumed to follow a uniform distribution and varied in the range of ±1‰. The mean and standard deviation of F_S were 0.167 and 0.003 mg $m^{-2}s^{-1}$, and those of F_P were -0.005 and 0.003 mg $m^{-2}s^{-1}$, respectively for the YRD, based on an ensemble of 10,000 simulations. For Nanjing, the mean ± standard deviation of F_S and F_P was 0.209 ± 0.024 and 0.086 ± 0.022 mg $m^{-2}s$, respectively. These mean flux values are essentially the same as those obtained with the default $\delta^{13}C_P$ and $\delta^{13}C_F$ values giving in Table 3 and the standard deviations represent uncertainties of the partitioned fluxes.

Another source of uncertainty in our flux partitioning analysis is related to human breath (Affek and Eiler 2006). Using the method of Prairie and Duarte (2007), we estimated that human respiration flux was 0.006 and 0.013 mg $m^{-2}s^{-1}$, or 3.7% and 11.65% of anthropogenic emission in the YRD and in Nanjing, respectively. The food diet in the region is predominantly C3 grains. By including this additional source in Equations 3 and 4 and by assuming that the isotopic signature of human respiration is the same as $\delta^{13}C_P$ shown in Table 3, F_S and F_P would increase by 0.008 and 0.001 mg $m^{-2}s^{-1}$ in the YRD and by 0.018 mg $m^{-2}s^{-1}$ and 0.005 mg $m^{-2}s^{-1}$ in Nanjing, respectively.

4.4 Comparison of the Miller-Tans and the Keeling method

By applying the Miller-Tans method to daytime and nighttime observations separately, we obtained the effective source signatures that are consistent with the inventory analysis for the YRD and for the Nanjing Municipality. The daytime measurement revealed that the sources were on average 0.46‰ more enriched in ^{13}C than the signature $\delta^{13}C_S$ obtained with the nighttime measurement. For comparison, the overall $\delta^{13}C_S$ of the anthropogenic sources in the YRD was also higher than that in Nanjing, the difference being 1.76‰ (Table 2). The interpretation that the daytime observations capture the influence of surface sources in the YRD region is supported by a trajectory analysis and by an analysis of the atmospheric methane to CO_2 emissions ratio observed at the same site (Shen et al. 2014). We note that the atmospheric measurements gave a smaller difference between the YRD and Nanjing than that obtained by the inventory data, likely because of different biological contributions between the two spatial scales.

We argue that Keeling plot method is not appropriate for daytime periods because the surface air is influenced by both the surface sources and by entrainment of the background air from above the boundary layer. If we applied the Keeling method to the daytime observations, the linear correlation coefficient was on average -0.898 which is weaker than the correlation coefficient obtained with the Miller-Tans method (-0.956). The resulting mean $\delta^{13}C_S$ would be 0.61‰ lower than the mean value shown in Figure 6. The difference in $\delta^{13}C_S$ between the YRD (daytime observations, Keeling method) and Nanjing (nighttime observations, Miller-Tans method) would become too small (0.15‰).

In comparison, the Keeling plot method showed reasonably good performance when applied to the nighttime observations. This is because surface inversion conditions effectively

prevented mixing of the free atmospheric air with the surface air, so that the single-source assumption implicit in the Keeling plot method was satisfied. If we applied Keeling plot method at monthly intervals to the nighttime data, the resulting $\delta^{13}C_S$ would decrease to -24.24‰ for Nanjing from -23.72‰, the value obtained with application of the Miller-Tans method to the nighttime observations.

5. Conclusion

We showed that the temporal changes of $\delta^{13}C$ followed the seasonal patterns of anthropogenic and biologic CO_2 emissions, with lower values in the winter than in the summer. An unusual feature that has not been seen in other urban environments is that the $\delta^{13}C$ exceeded that of the background atmosphere in some of the summer months. The highest monthly ^{13}C was -7.44‰ observed in July 2013, which was 0.74‰ greater than the WLG value for the same month. Evidence points to cement production as the key reason for why the atmospheric $\delta^{13}C$ was higher than at the background site. In contrast to the ^{13}C signal, the CO_2 mole fraction displayed very weak seasonality (July to January difference 15.6 ppm).

We hypothesized that the Miller-Tans method applied to the daytime and nighttime observations should yield the effective isotopic signature of surface sources at the regional (YRD) and the local (Nanjing) scale, respectively. According to the results of the Miller-Tans method, the effective source signal in the YRD was -23.25‰, which was 0.46‰ higher than that in the Nanjing Municipality. These results were consistent with inventory estimates of anthropogenic source signatures at these two spatial scales.

By combining inventory data on anthropogenic C sources and the atmospheric measurement of CO_2 mole fraction and its ^{13}C composition in an isotopic partitioning framework, we inferred that natural ecosystems in the YRD were a negligibly small sink of atmospheric CO_2, with an average flux of -0.009 mg $m^{-2}s^{-1}$. The Carbon Tracker inverse analysis also reveals a small annual mean daytime biological flux (-0.014 mg $m^{-2}s^{-1}$) for this region.

Data availability：

The atmospheric data are available upon request and from the Yale-NUIST Center website http://yncenter.sites.yale.edu/publications.

Acknowledgments:

This research was supported by the National Natural Science Foundation of China (Grant 41475141, 41505005), the U. S. National Science Foundation (Grant 1520684), the Ministry of Education of China (Grant PCSIRT), and the Priority Academic Program Development of Jiangsu Higher Education Institutions (Grant PAPD). The first author also acknowledged a visiting scholarship from China Scholarship Council and a Graduate Student Innovation Grant from Jiangsu Provincial Government (Grant KYLX_0848).

References

Affek, H. P., Eiler, J. M. (2006). Abundance of mass 47 CO2 in urban air, car exhaust, and human breath. Geochimica et Cosmochimica Acta **70**(1): 1-12.

Akbari H, Menon S, Rosenfeld A. Global cooling: increasing world-wide urban albedos to offset CO2. Climatic Change, 2009, **94**(3-4): 275-286.

Andres, R. J., Marland, G., Boden, T., Bischof, S. (1994). Carbon dioxide emissions from fossil fuel consumption and cement manufacture, 1751-1991; and an estimate of their isotopic composition and latitudinal distribution, Oak Ridge National Lab., TN (United States);

Bai, Y., (2011) A comparative study on turbulent fluxes exchange over Nanjing urban and suburban in summer. (in Chinese) Nanjing, Nanjing University of Information Science & Technology.

Ballantyne, A. P., Miller, J. B., Baker, I. T., Tans, P. P., White, J. W. C. (2011). Novel applications of carbon isotopes in atmospheric CO2: what can atmospheric measurements teach us about processes in the biosphere?. Biogeosciences, 8(10), 3093-3106.

Ballantyne, A. P., Miller, J. B., Tans, P. P. (2010). Apparent seasonal cycle in isotopic discrimination of carbon in the atmosphere and biosphere due to vapor pressure deficit. Global Biogeochemical Cycles, 24(3), 1-16.

Bi, J., Zhang, R., Wang, H., Liu, M.,Wu, Y. (2011). The benchmarks of carbon emissions and policy implications for China's cities: Case of Nanjing. Energy Policy **39**(9): 4785-4794.

Bowling, D. R., Sargent, S. D., Tanner, B. D., and Ehleringer, J. R. (2003). Tunable diode laser absorption spectroscopy for stable isotope studies of ecosystem–atmosphere CO2 exchange, Agric. Forest Meteorol. **118:** 1–19.

Bush, S. E., Pataki, D.E., Ehleringer, J.R. (2007). Sources of variation in δ13C of fossil fuel emissions in Salt Lake City, USA. Applied Geochemistry **22**(4): 715-723.

CESY (2013). China Energy Statistical Yearbook 2013: China Statistical Publishing House, Beijing. (in Chinese) Also available at: <http://www.stats.gov.cn/tjsj/ndsj/ 2013/indexch.htm>.

Clark-Thorne, S. T., C. J. Yapp (2003). Stable carbon isotope constraints on mixing and mass balance of CO2 in an urban atmosphere: Dallas metropolitan area, Texas, USA. Applied Geochemistry **18**(1): 75-95.

Coutts, A. M., Beringer, J., Tapper, N.J. (2007). Characteristics influencing the variability of urban CO2 fluxes in Melbourne, Australia. Atmospheric Environment **41**(1): 51-62.

China Cement: http://hy.ccement.com/map/, last access: 6 July 2016 (in Chinese).

CSY (2013). China Statistical Yearbook. National Bureau of Statistics of China. (in Chinese) Also available at: <http://www.stats.gov.cn/tjsj/ndsj/2013/indexch.htm>

Duan Y. (1995) Study of characteristics of coal isotope conposition in China Coal Geology & Exploration **23**(1) 29-33.

Ehleringer, J.R., Bowling, D.R., Flanagan, L.B., Fessenden, J.,Helliker, B., Martinelli, L.A., Ometto, J.P. (2002). Stable isotopes and carbon cycle processes in forests and grasslands. Plant biology **4**(2): 181-189.

Farquhar, G., J. Lloyd (1993). Carbon and oxygen isotope effects in the exchange of carbon dioxide between terrestrial plants and the atmosphere. Stable isotopes and plant carbon-water relations **40**: 47-70.

Fessenden, J. E., J. R. Ehleringer (2002). Age-related variations in δ13C of ecosystem respiration across a coniferous forest chronosequence in the Pacific Northwest. Tree Physiology **22**(2-3): 159-167.

Friedman, L., A. P. Irsa (1967). Variations in isotopic composition of carbon in urban atmospheric carbon dioxide. Science **158**(3798): 263-264.

Gorski G, Strong C, Good S P, Bares,R.,Ehleringer,J.R.,Bowen,G.J.. Vapor hydrogen and oxygen isotopes reflect water of combustion in the urban atmosphere. Proceedings of the National Academy of Sciences, 2015, **112**(11): 3247-3252.

Griffis, T. J., Lee, X., Baker, J.M., Sargent, S.D., King, J.Y. (2005). Feasibility of quantifying ecosystem–atmosphere C18O16O exchange using laser spectroscopy and the flux-gradient method. Agricultural and Forest Meteorology **135**(1-4): 44-60.

Griffis, T J. (2013). Tracing the flow of carbon dioxide and water vapor between the biosphere and atmosphere: A review of optical isotope techniques and their application. Agricultural and Forest Meteorology, **174**:85-109.

Guha, T., P. Ghosh (2010). Diurnal variation of atmospheric CO2 concentration and delta C-13 in an urban atmosphere during winter-role of the Nocturnal Boundary Layer. Journal of Atmospheric Chemistry **65**(1): 1-12.

Guha, T. and P. Ghosh (2015). Diurnal and seasonal variation of mixing ratio and delta C-13 of air CO2 observed at an urban station Bangalore, India. Environmental Science and Pollution Research **22**(3): 1877-1890.

Helfter, C., Famulari, D., Phillips, G.J., Barlow, J.F., Wood, C.R.,Grimmond, C.S.B., Nemitz, E. (2011). Controls of carbon dioxide concentrations and fluxes above central London. Atmospheric Chemistry and Physics **11**(5): 1913-1928.

ICLEI (International Council for Local Environmental Initiatives). (2008). Local government operations protocol for the quantification and reporting of greenhouse gas emissions inventories. [Available online at http://www.arb.ca.gov/cc/protocols/localgov/archive/final lgo protocol 2008–09–25.pdf.]

Idso, S. B., Idso, C.D., Balling, R.C. (2002). Seasonal and diurnal variations of near-surface atmospheric CO 2 concentration within a residential sector of the urban CO 2 dome of Phoenix, AZ, USA. Atmospheric Environment **36**(10): 1655-1660.

Jasek, A., Zimnoch, M., Gorczyca, Z., Smula, E.,Rozanski, K. (2014). Seasonal variability of soil CO2 flux and its carbon isotope composition in Krakow urban area, Southern Poland. Isotopes in Environmental and Health Studies **50**(2): 143-155.

Keeling, C. D. (1958). The concentration and isotopic abundances of atmospheric carbon dioxide in rural areas. Geochimica et Cosmochimica Acta **13**(4): 322-334.

Keeling, C. D. (1961). The concentration and isotopic abundances of carbon dioxide in rural and marine air. Geochimica et Cosmochimica Acta **24**(3): 277-298.

Koerner, B., J. Klopatek (2002). Anthropogenic and natural CO2 emission sources in an arid urban environment. Environmental Pollution **116**: S45-S51.

Leavitt, S. W., Paul, E.A., Galadima, A.,Nakayama, F.S., Danzer, S.R., Johnson, H., Kimball, B.A. (1995). Carbon isotopes and carbon turnover in cotton and wheat FACE experiments. Plant and Soil **187**(2): 147-155.

Lichtfouse, E., Lichtfouse, M., Jaffrezic, A. (2003). delta C-13 values of grasses as a novel indicator of pollution by fossil-fuel-derived greenhouse gas CO2 in urban areas. Environmental Science & Technology **37**(1): 87-89.

Liu, H., Feng, J., Järvi, L., Vesala, T. (2012). Four-year (2006–2009) eddy covariance measurements of CO2 flux over an urban area in Beijing. Atmospheric Chemistry and Physics **12**(17): 7881-7892.

Lloyd, J., Kruijt, B., Hollinger, D.Y., Grace, J., Francey, R.J., Wong, S., Kelliher, F.M., Miranda, A.C., Farquhar, G.D., Gash, J.H.C. (1996). Vegetation effects on the isotopic

composition of atmospheric CO2 at local and regional scales: theoretical aspects and a comparison between rain forest in Amazonia and a boreal forest in Siberia. Functional Plant Biology **23**(3): 371-399.

Lloyd, J., Francey, R.J., Mollicone, D., Raupach, M.R, Sogachev, A., Arneth, A., Byers, J.N., Kelliher, F.M., Rebmann, C., Valentini, R. (2001). Vertical profiles, boundary layer budgets, and regional flux estimates for CO2 and its 13C/12C ratio and for water vapor above a forest/bog mosaic in central Siberia. Global Biogeochemical Cycles **15**(2): 267-284.

McDonald, B.C., McBride, Z. C., Martin, E. W., Harley, R. A. High-resolution mapping of motor vehicle carbon dioxide emissions. Journal of Geophysical Research: Atmospheres, 2014, **119**(9): 5283-5298.

McManus, J. B., Zahniser, M.S., Nelson, D.D., Williams, L.R., Kolb, C.E. (2002). Infrared laser spectrometer with balanced absorption for measurement of isotopic ratios of carbon gases. Spectrochimica Acta Part A: Molecular and Biomolecular Spectroscopy **58**(11): 2465-2479.

Miller, J. B., P. P. Tans (2003). Calculating isotopic fractionation from atmospheric measurements at various scales. Tellus B **55**(2): 207-214.

Miller, J.B., Tans, P.P., White, J.W.C., Conway, T.J., Vaughn, B.W. (2003). The atmospheric signal of terrestrial carbon isotopic discrimination and its implication for partitioning carbon fluxes. Tellus B **55**(2): 197-206.

Newman, S., Xu, X., Gurney, K.R., Hsu, Y.K., Li, K.F., Jiang, X., Keeling, R., Feng, S., O'Keefe, D., Patarasuk, R. and Wong, K.W. (2016). Toward consistency between trends in bottom-up CO2 emissions and top-down atmospheric measurements in the Los Angeles megacity. Atmospheric Chemistry and Physics, 16(6):3843-3863.

Moore J., Jacobson A.D. (2015). Seasonally varying contributions to urban CO2 in the Chicago, Illinois, USA region: Insights from a high-resolution CO2 concentration and d13C record. Elementa: Science of the Anthropocene **3**, 000052.

Mu, H., Li, H., Zhang, M., Li, M. (2013). Analysis of China's carbon dioxide flow for 2008. Energy Policy **54**: 320-326.

Newman, S., Xu, X., Affek, H.P., Stolper, E., Epstein, S. (2008). Changes in mixing ratio and isotopic composition of CO2in urban air from the Los Angeles basin, California, between 1972 and 2003. Journal of Geophysical Research **113**(D23) : 1-15.

NSY (2013). Nanjing Statistical Yearbook. Nanjing Municipal Bureau Statistics. (in Chinese) Also available at: < http://www.njtj.gov.cn/2004/2013/renmin/index.htm>

Ometto, J. P., Flanagan, L.B., Martinelli, L.A., Moreira, M.Z., Higuchi, N., Ehleringer, J.R. (2002). Carbon isotope discrimination in forest and pasture ecosystems of the Amazon Basin, Brazil. Global Biogeochemical Cycles **16**(4):1-10.

Ometto, J.P., Ehleringer, J.R., Domingues, T.F., Berry, J.A., Ishida, F.Y., Mazzi, E., Higuchi, N., Flanagan, L.B., Nardoto, G.B., Martinelli, L.A. (2006). The stable carbon and nitrogen isotopic composition of vegetation in tropical forests of the Amazon Basin, Brazil. Biogeochemistry **79**(1-2): 251-274.

Pang, J., Wen, X., Sun, X. (2016). Mixing ratio and carbon isotopic composition investigation of atmospheric CO2 in Beijing, China. Sci Total Environ **539**: 322-330.

Pataki, D. E. (2005). Can carbon dioxide be used as a tracer of urban atmospheric transport? Journal of Geophysical Research **110**(D15102) : 1-8.

Pataki, D. E., Bowling, D.R., Ehleringer, J.R. (2003). Seasonal cycle of carbon dioxide and its isotopic composition in an urban atmosphere: Anthropogenic and biogenic effects. Journal of Geophysical Research-Atmospheres **108**(D23) : 1-8.

Pataki, D. E., Bowling, D.R., Ehleringer, J.R., Zobitz, J.M. (2006). High resolution atmospheric monitoring of urban carbon dioxide sources. Geophysical Research Letters **33**(3) : 1-5.

Pataki, D. E., Ehleringer, J.R., Flanagan, L.B., Yakir, D., Bowling, D.R., Still, C.J., Buchmann, N., Kaplan, J.O., Berry, J.A. (2003). The application and interpretation of Keeling plots in terrestrial carbon cycle research. Global Biogeochemical Cycles **17**(1): 1-14

Pataki, D. E., Lai, C., Keeling, C.D., Ehleringer, J.R. (2007). Insights from stable isotopes on the role of terrestrial ecosystems in the global carbon cycle. Terrestrial Ecosystems in a Changing World, Springer**:** 37-44.

Pataki,D.E., Emmi,P.C., Forster,C.B., Mills,J.I., Pardyjak,E.R., Peterson,T.R., Thompson,J.D., Dudley-Murphy,E., An integrated approach to improving fossil fuel emissions scenarios with urban ecosystem studies. Ecological Complexity, 2009, **6**(1): 1-14.

Pataki, D. E., Xu, T., Luo, Y.Q., Ehleringer, J.R. (2007). Inferring biogenic and anthropogenic carbon dioxide sources across an urban to rural gradient. Oecologia **152**(2): 307-322.

Peters,W., Jacobson,A.R., Sweeney,C., Andrews,A.E., Conway,T.J., Masarie,,K., Miller,J.B., Bruhwiler,L.M., Petron,G., Hirsch, A.I., Worthy,D.E., van der Werf,G.R., Randerson,J.T., Wennberg,P.O., Krol,M.C., Tans,P.P., An atmospheric perspective on North American carbon dioxide exchange: CarbonTracker.Proceedings of the National Academy of Sciences, 2007, **104**(48): 18925-18930.

Prairie, Yves T., and Carlos M. Duarte. (2007). Direct and indirect metabolic CO_2 release by humanity. Biogeosciences 4(2): 215-217.

Rella, C. (2011). Accurate stable carbon isotope ratio measurements with rapidly varying carbon dioxide concentrations using the Picarro δ13C G2101-i gas analyzer, Picarro White Paper. Picarro Inc.

Ren, L., Wang, W., Wang, J., Liu, R. (2015). Analysis of energy consumption and carbon emission during the urbanization of Shandong Province, China. Journal of Cleaner Production **103**: 534-541.

Rose L S, Akbari H, Taha H. Characterizing the fabric of the urban environment: a case study of Greater Houston, Texas. Lawrence Berkeley National Laboratory, 2003.

Satterthwaite D. Cities' contribution to global warming: notes on the allocation of greenhouse gas emissions. Environment and Urbanization, 2008, **20**(2): 539–549.

Shen, S., Yang, D., Xiao, W., Liu, S., Lee, X. (2014). Constraining anthropogenic CH4 emissions in Nanjing and the Yangtze River Delta, China, using atmospheric CO2 and CH4 mixing ratios. Advances in Atmospheric Sciences **31**(6): 1343-1352.

Song, T., Wang Y. (2012). Carbon dioxide fluxes from an urban area in Beijing. Atmospheric Research **106**: 139-149.

Sun, B., Dilcher, D.L., Beerling, D.J., Zhang, C., Yan, D., Kowalski, E. (2003). Variation in Ginkgo biloba L. leaf characters across a climatic gradient in China. Proceedings of the National Academy of Sciences **100**(12): 7141-7146.

Takahashi, H. A., Konohira, E., Hiyama, T., Minami, M., Nakamura, T., Yoshida, N. (2002). Diurnal variation of CO2 concentration, Delta C-14 and delta C-13 in an urban forest: estimate of the anthropogenic and biogenic CO2 contributions. Tellus B **54**(2): 97-109.

Tans, P. (1981). 13C/12C of industrial C02. In SCOPE 16: Carbon Qcle Modelling (B.Bolin, ed.), John Wiley and Sons, Chichester, England, 127-129.

Thoning, K. W., Tans, P.P., Komhyr, W.D. (1989). Atmospheric carbon dioxide at Mauna Loa Observatory: 2. Analysis of the NOAA GMCC data, 1974–1985. Journal of Geophysical Research: Atmospheres (1984–2012) **94**(D6): 8549-8565.

Turnbull, J. C., Sweeney, C., Karion, A., Newberger, T., Lehman, S. J., Tans, P.P., Davis, K.J., Lauvaux, T., Miles, N.L., Richardson, S.J., Cambaliza. (2015). Toward quantification and source sector identification of fossil fuel CO2 emissions from an urban area: Results from the INFLUX experiment. Journal of Geophysical Research: Atmospheres,120(1), 292-312.

Wada, R., Nakayama, T., Matsumi, Y., Hiyama, T., Inoue, G., Shibata, T. (2011). Observation of carbon and oxygen isotopic compositions of CO2 at an urban site in Nagoya using Mid-IR laser absorption spectroscopy. Atmospheric Environment **45**(5): 1168-1174.

Wang, W. , D. E. Pataki (2012). Drivers of spatial variability in urban plant and soil isotopic composition in the Los Angeles basin. Plant and Soil **350**(1-2): 323-338.

Wen, X. F., Meng, Y., Zhang, X., Sun, X., Lee, X. (2013). Evaluating calibration strategies for isotope ratio infrared spectroscopy for atmospheric $^{13}CO_2/^{12}CO_2$ measurement. Atmospheric Measurement Techniques Discussions **6**(1): 795-823.

Widory, D. (2006). Combustibles, fuels and their combustion products: A view through carbon isotopes. Combustion Theory and Modelling **10**(5): 831-841.

Widory, D., M. Javoy (2003). The carbon isotope composition of atmospheric CO2 in Paris. Earth and Planetary Science Letters **215**(1-2): 289-298.

Yakir, D., L. da SL Sternberg (2000). The use of stable isotopes to study ecosystem gas exchange. Oecologia **123**(3): 297-311.

Yang, H.M., Wang, H.Z. , Wu, Y.B. (2011). Observation and characteristics analysis of traffic flow in Nanjing. (in Chinese) Environmental Science and Technology **24**(2): 98-101.

Zimnoch, M., Florkowski, T., Necki, J., Neubert, R. (2004). Diurnal variability of delta C-13 and delta O-18 of atmospheric CO2 in the urban atmosphere of Krakow, Poland. Isotopes in Environmental and Health Studies **40**(2): 129-143.

Zobitz, J. M., Burns, S.P., Reichstein, M., Bowling, D.R. (2008). Partitioning net ecosystem carbon exchange and the carbon isotopic disequilibrium in a subalpine forest. Global Change Biology **14**(8): 1785-1800.

Zondervan, A., H. A. Meijer (1996). Isotopic characterisation of CO2 sources during regional pollution events using isotopic and radiocarbon analysis. Tellus B **48**(4): 601-612.

Zhou, L., Conway, T.J., White, J.W., Mukai, H., Zhang, X., Wen, Y., Li, J. and MacClune, K., (2005). Long‐term record of atmospheric CO2 and stable isotopic ratios at Waliguan Observatory: Background features and possible drivers, 1991–2002. Global Biogeochemical Cycles, **19**(3).

839 **Figure 1**. Dependence of the observed $\delta^{13}C$ on the H_2O mole fraction. The lines represent
840 Equation 2. Error bars are ± one standard deviation. The data in the left panel was obtained
841 on October 1, 2014 using a 439-ppm standard gas and the true $\delta^{13}C$ value of -32.8‰, and that
842 in the right panel on June 10, 2015 using a 488-ppm standard gas and the true $\delta^{13}C$ value of -
843 34.1‰.

844

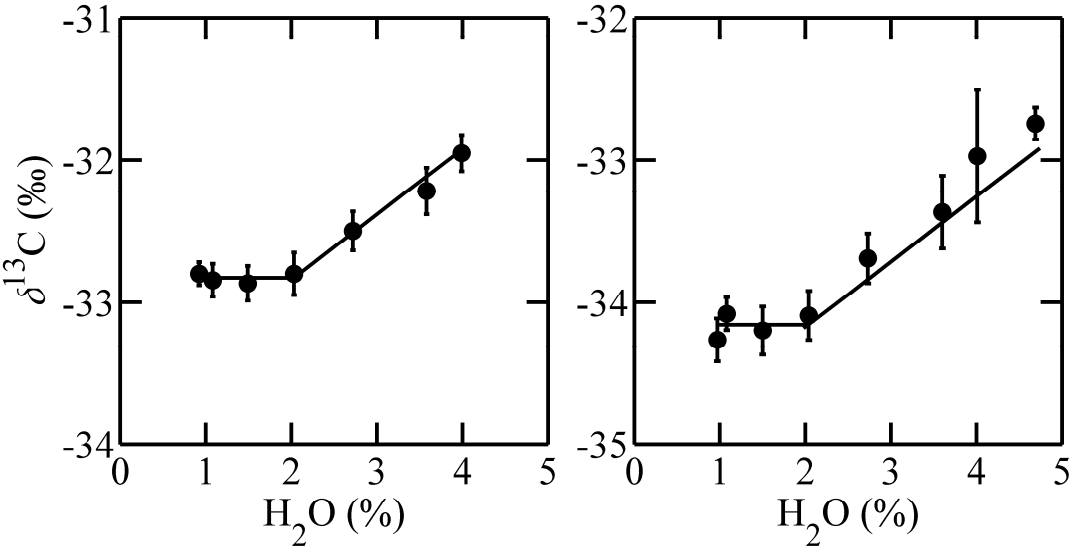

845

Figure 2. Monthly total CO_2 mole fraction (upper panel) and $\delta^{13}C$ (lower panel): Solid lines with circles: whole-day means; dashed lines with up triangles: daytime (10:00-16:00) means; dashed line with down triangles: nighttime (22:00-6:00) means; smooth solid lines, monthly means observed at WLG.

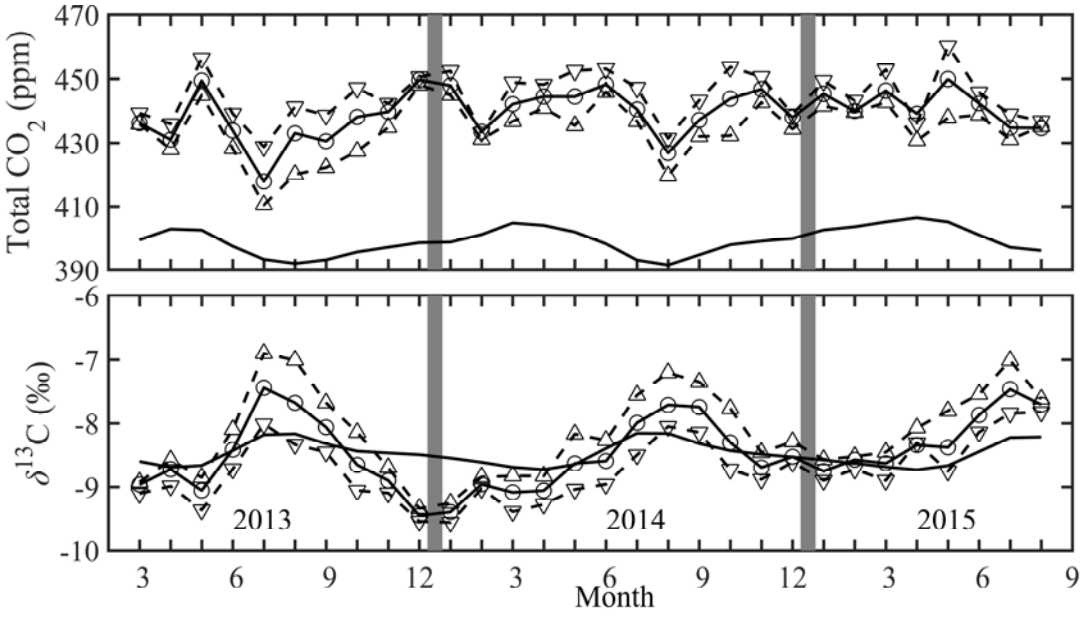

853 **Figure 3**. Mean diurnal variation of the CO_2 mole fraction (upper panels) and the $\delta^{13}C$ value

854 (bottom panels) between March, 2013 and August, 2015.

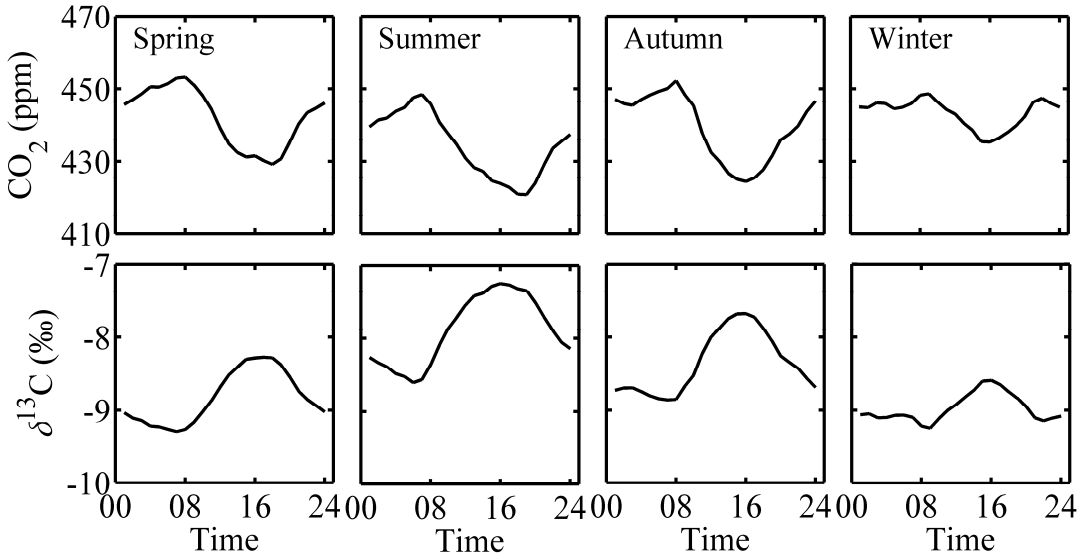

855

856

857 **Figure 4**. Application of the Miller-Tans method to all valid daytime (10:00-16:00) data
858 obtained between March, 2013 and August, 2015. Each data point is one hourly mean. The
859 solid line is the geometric mean regression according to Equation 1. Errors bounds on the
860 regression coefficient are 95% confidence interval.

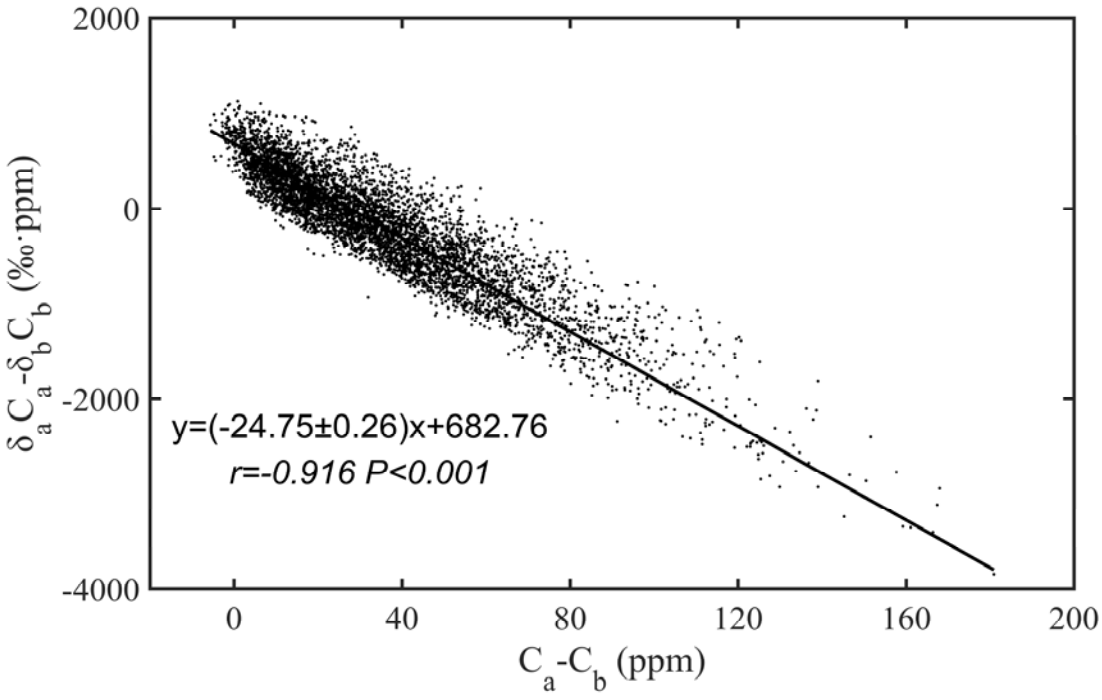

861

862

863

Figure 5. Same as Figure 4 but for nighttime (22:00-6:00) data.

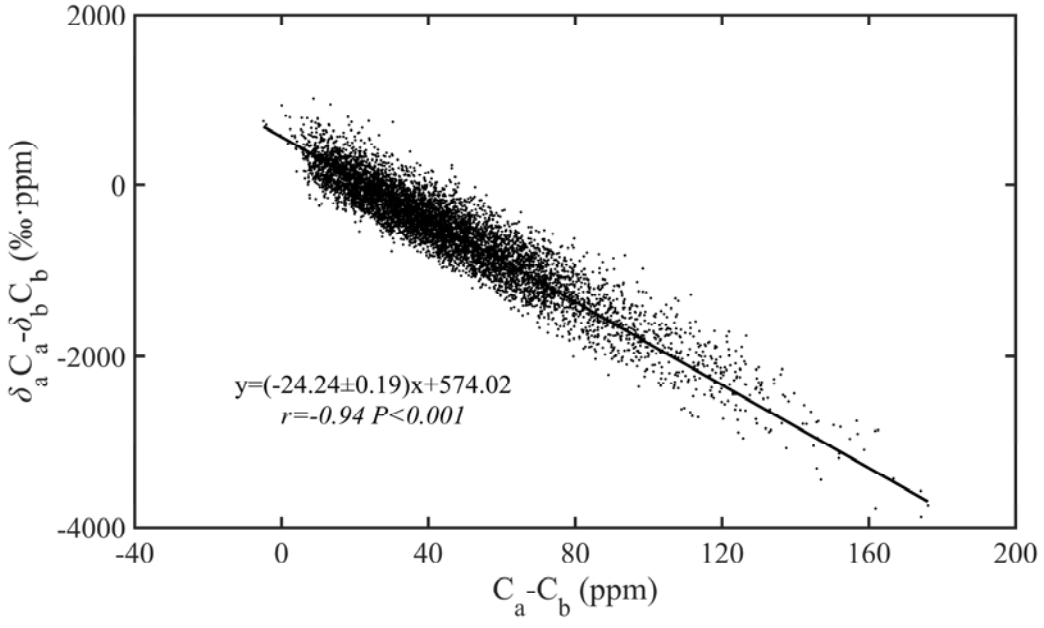

Figure 6. Time series of monthly ^{13}C signature of surface sources in the YRD (black line) and in Nanjing (grey line), obtained from daytime and nighttime measurement, respectively. The error bars are ± one standard deviation of the Miller-Tans regression.

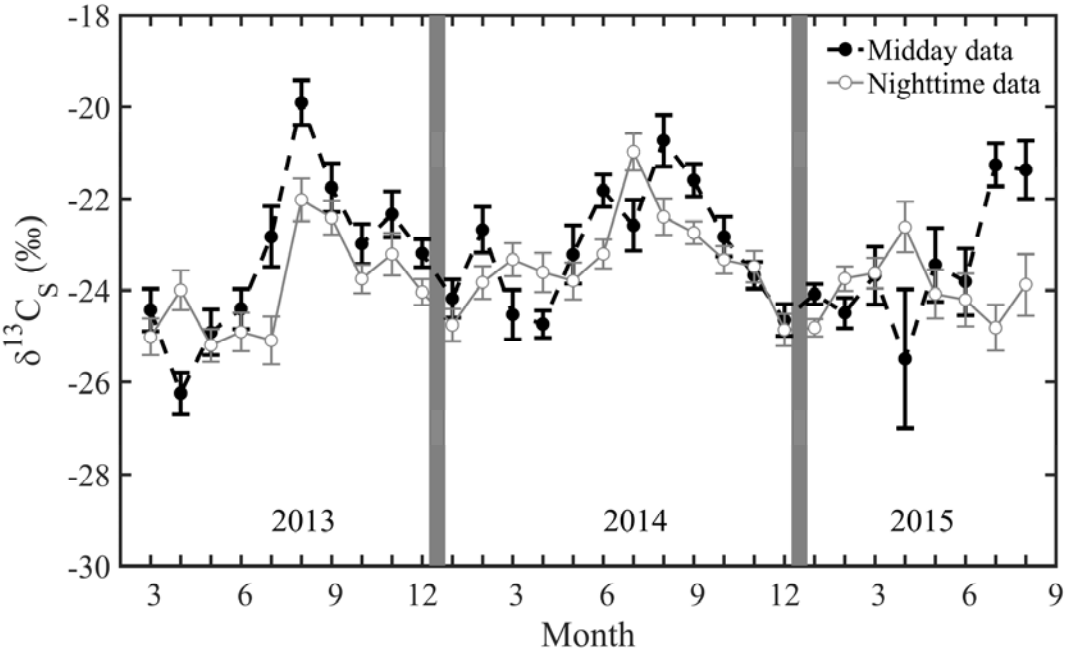

Figure 7. Time series of monthly net surface CO_2 flux (F_S), biological CO_2 flux (F_P), anthropogenic CO_2 flux excluding cement emission (F_F) and cement CO_2 flux (F_c) in the YRD. All the fluxes are in mg $m^{-2}s^{-1}$. The results are based on the source signature derived from daytime atmospheric measurements.

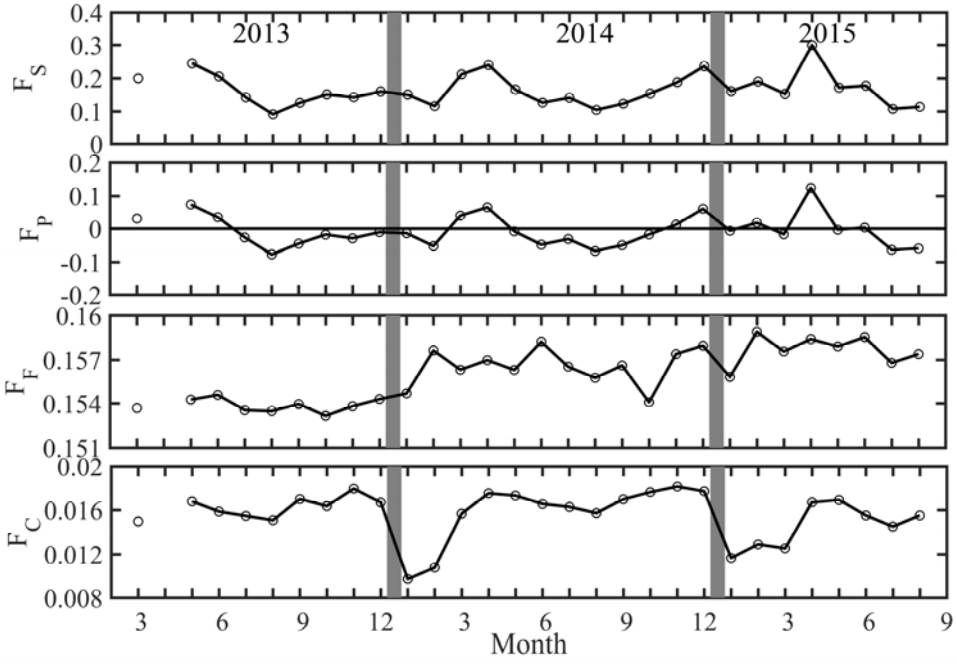

Figure 8. Time series of monthly net surface CO_2 flux (F_S), biological CO_2 flux (F_P), anthropogenic CO_2 flux excluding cement emission (F_F) and cement CO_2 flux (F_c) in the Nanjing. All the fluxes are in mg $m^{-2}s^{-1}$. The results are based on the source signature derived from nighttime atmospheric measurements.

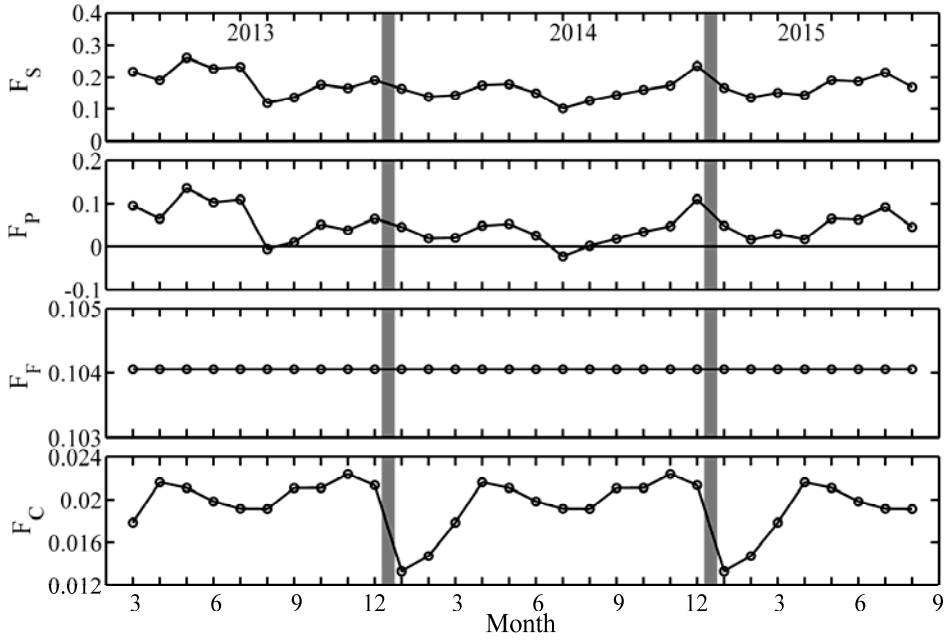

890 **Table 1** Standard gases used for instrument calibration.

ID	CO_2 (ppm)	$\delta^{13}C$ (‰)	Period
1 Low	381.89	-29.75	Mar, 2013 - Aug, 2014
1 High	502.35	-30.01	Mar, 2013 - Aug, 2014
2 Low	380.92	-29.75	Sep, 2014 - Aug, 2015
2 High	501.05	-30.01	Sep, 2014 - Aug, 2015

891

892 **Table 2** Percentage of "fossil-plus" sources and their $\delta^{13}C$ values for the YRD and Nanjing.

	Percentage (%)		$\delta^{13}C$ (‰)		
Sources	YRD	Nanjing	YRD	Nanjing	References
Coal	70.0	52.3	-25.46	-25.46	Duan 1995, Widory 2006
Gasoline	2.1	11.4	-28.80	-28.80	Widory and Javoy 2003
Diesel	3.2	1.6	-29.80	-29.80	Widory 2006
Fuel oil	2.1	0.3	-28.93	-28.93	Widory and Javoy 2003
Natural gas	2.7	5.0	-39.50	-39.50	Pang et al. 2016
LPG	0.7	0.2	-31.70	-31.70	Widory 2006
Pig iron	8.7	12.7	-24.58	-24.58	this study
Crude steel	1.5	0.7	-24.82	-24.82	this study
Ammonia synthesis	9.0	15.9	-28.50	-28.50	this study
Total	100	100	-26.07	-26.42	

893

894 **Table 3**. Inventory data for the isotopic composition of surface CO_2 sources and their
895 percentage of contribution in the YRD and in Nanjing. Here the "fossil-plus" category
896 includes all non-cement anthropogenic emissions listed in Table 2.

Sources	YRD		Nanjing	
	$\delta^{13}C$ (‰)	Percentage (%)	$\delta^{13}C$ (‰)	Percentage (%)
"Fossil-plus"	-26.07	91.0	-26.42	96.4
Cement	0.20	9.0	0.20	3.6
Anthropogenic	-23.71	100	-25.47	100
Biological	-28.2	——	-28.2	——

897